Soft Matter

PAPER

View Article Online
View Journal | View Issue

Cite this: *Soft Matter*, 2026, **22**, 1425

Synthesis of single chain polystyrene nanoparticles *via* reversible ionic interactions

Anastasia Stergiou, Marileta Tsakanika and Georgios Sakellariou *

Advances in polymer science have enabled the synthesis of complex macromolecular structures, inspired by the defined sequences found in natural molecules, such as proteins. In this light, the development of single-chain nanoparticle (SCNP) polymeric systems is currently being intensively investigated. These nanoparticles are formed through self-folding of the polymer chain at specified sites and depending on the nature of the bonds, a dynamic system can be developed. Intramolecular networking through dynamic bonds, such as interactions between ionic dipoles, allows for a change in nanoparticle configuration in response to external stimuli. In this study, polystyrene-based SCNPs synthesized through the development of ionic interactions are presented. Controlled radical RAFT polymerization was carried out for the synthesis of linear polystyrene chains containing 4-vinylpyridine monomer units at a 1–3% molar ratio. Through reaction with 1,3-propanesultone, the 4-vinylpyridine monomer serves as the site for the introduction of ionic dipoles into the polymer chain *via* the quaternization of pyridine nitrogen. In the presence of a nonpolar solvent, the ionic dipoles subsequently attract each other, forming reversible intramolecular cross-links along the polymer chain. The molecular weight and polydispersity of the polymeric samples were evaluated by size exclusion chromatography, while the percentage of 4-vinylpyridine and ion pairs incorporated into the polymer chain was determined by ^{1}H-NMR spectroscopy measurements. Differential scanning calorimetry (DSC) was employed to examine the thermal properties of the linear polymer chain compared to the forming network. Additionally, viscosity and dynamic light scattering (DLS) measurements were performed to verify network formation, by comparing the intrinsic viscosity and hydrodynamic radius of the linear and cross-linked samples.

Received 19th November 2025,
Accepted 16th January 2026

DOI: 10.1039/d5sm01159k

rsc.li/soft-matter-journal

Introduction

Developments in polymer science over recent decades have facilitated the advancement of new methodologies for synthesizing polymers with complex macromolecular architectures. The interest in developing linear polymeric chains that permit further development of complex macromolecular architectures is noteworthy.[1] Biological macromolecules such as proteins and enzymes attract research interest due to the strictly defined sequence of just 20 amino acids in their primary structure, which, in turn, govern the secondary and tertiary structure, leading to perfectly defined self-organized quaternary structures.[2–6] Since the synthesis of well-defined and functional three-dimensional structures with uniform polydispersity, like proteins, has not, to our knowledge, been achieved, efforts are focused on synthesizing polymeric systems that have self-folding properties, due to the active groups they carry.[3,7,8]

By emulating nature's precision in constructing functional three-dimensional architectures, researchers have turned their attention to single-chain nanoparticles (SCNPs) as a promising model for achieving similar self-organizing capabilities in synthetic systems. These nanoparticles are well-defined polymeric systems in terms of size and arrangement of functional groups on the linear precursor and have been synthesized through intramolecular cross-linking (Scheme 1),[9–12] as first reported by Kuhn and Balmer in 1955.[13] The size of the nanoparticles formed is determined by the length of the linear precursor chain and the percentage of cross-linkers.[10,11]

Widely used techniques for the development of such systems include "click" chemistry, Friedel–Crafts alkylation, radical coupling, photochemical or thermal cycloadditions, the development of disulfide bonds,[14,15] *etc.*[2,9,16] These post-polymerization cross-linking reactions are favored due to their high efficiency, selectivity, and minimal side reactions, which are essential criteria for their selection in SCNP formation.[1,2] Typical examples of SCNP applications are their use in nanomedicine, sensors and catalytic systems, self-healing systems, electro–optical devices, viscosity modifiers, and eye lens implants.[1,3,7,9,10,12,14–18]

Polymer chain networking can be achieved through the formation of either reversible or irreversible covalent bonds (*e.g.* imine bonds and disulfide bonds[19]) or non-covalent

Laboratory of Industrial Chemistry, Department of Chemistry, National and Kapodistrian University of Athens, Panepistimiopolis Zografou, 15771, Athens, Greece. E-mail: gsakellariou@chem.uoa.gr

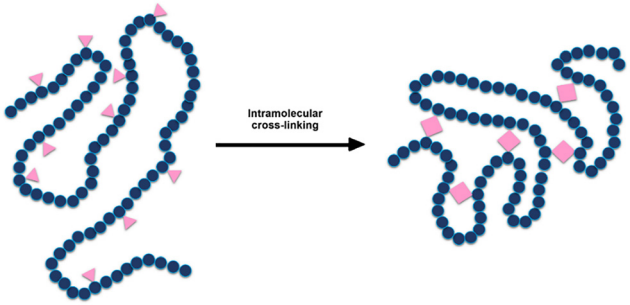

Scheme 1 Representation of intramolecular chain folding, through cross-linking.

interactions (*e.g.* hydrogen bonding, π–π stacking, metal coordination, and hydrophobic interactions).[1,7,9,10,14–16] These bonds govern the stability and responsiveness of the resulting nanoparticles. Nanoparticles cross-linked by irreversible covalent bonds tend to remain stable under external stimuli, whereas those connected by reversible bonds can undergo reversible collapse and reshaping in response to environmental changes such as the presence of oxidizing or reducing agents, fluctuations in pH or temperature, and specific wavelengths of radiation (λ). Since the mid-1990s, the variety of chemical reactions available for post-polymerization modification has increased due to the development of controlled/living radical polymerization techniques (RAFT, ATRP, and NMP). These techniques allow the facile synthesis of polymers with controlled architectures, exhibiting polydispersity indices close to those of well-defined anionic "living" polymers.[3,7]

Zwitterionic polymers are a class of macromolecules characterized by the presence of both positively and negatively charged functional groups within the same repeating structural unit. Depending on the anionic group, polyamphoteric materials – also referred to as polybetaines – can be categorized into poly(carboxybetaine), poly(phosphobetaine), or poly(sulfobetaine).[20–22] The coexistence of positive and negative charges within the same monomer unit imparts hydrophilic properties to the polymer, allowing for the synthesis of materials with excellent dipole torque and high ionic conductivity due to the number of charges present. Their dynamic nature enables the formation of dynamic polymeric systems, where their morphology is influenced by the surrounding environment. These systems can react to external stimuli such as changes in the salt ion concentration or solvent polarity.[20–22] These polymers find broad applications across diverse fields including oil recovery, cosmetics, catalysis, water desalination, artificial leather for robotics, and cryoprotectors and as components in flexible materials intended to replace carbon-based counterparts, where optical transparency is critical and carbon's black color limits such applications.[4,22–25]

Single-chain polymer nanoparticles consist of intramolecular loops, particularly prominent when the degree of cross-linking is low. Their viscoelastic behavior can be tuned, depending on the desired application. Thus, SCNP nanocomposites with linear polymer chains are of great interest. In particular, ultra-small crosslinked polymeric particles with tailored softness have been reported to significantly decrease the viscosity of all-polymer nanocomposites,[26,27] in contrast to Einstein's viscosity law.[28] More recently, the addition of varying amounts of SCNPs to entangled linear polymer chains led to increased viscosity in the all-polymer nanocomposites with the SCNP content lower than 20 wt%.[29]

Literature highlights instances where the reversible formation of SCNPs is influenced by the surrounding environment during crosslinking. Terashima *et al.*[30] synthesized methacrylate-based/PEGMA random amphiphilic copolymers designed to facilitate SCNP formation *via* reversible hydrophobic interactions in aqueous media. Various characterization techniques, including multi-angle laser light scattering coupled with SEC (SEC-MALLS) and DLS, were employed to investigate the development of intramolecular interactions. SEC-MALLS measurements, performed in DMF and water, revealed that polymer chains exist as unimers in DMF, whereas in water, polymers with a methacrylate monomer content up to 40 mol% underwent dynamic intramolecular crosslinking. At higher concentrations exceeding 50%, multichain aggregates were observed. DLS measurements in various solvents demonstrated that in good organic solvents, such as chloroform ($CHCl_3$) and dimethyl formamide (DMF), polymer chain conformation remained unaffected by the monomer composition. Furthermore, the alkyl side chain length played a significant role in determining the final structure. Longer alkyl groups enhanced single-chain folding efficiency, leading to a decreased nanoparticle radius, especially for methacrylate monomer contents up to 40 mol%. Artar *et al.*[31] synthesized two types of methacrylate-based amphiphilic polymers using RAFT polymerization, differing in their selectivity within a hydrophobic environment. Their objective was to design selective dynamic SCNPs capable of encapsulating a non-selective active catalytic center, Ru(II), in an aqueous environment through hydrophobic interactions. Inductively coupled plasma–atomic emission spectroscopy (ICP–AES) measurements revealed that each polymer chain incorporated 2–3 Ru centers, while DLS results confirmed nanoparticle formation, with a slight decrease in the hydrodynamic radius, preserving the system's single-chain characteristics. Similarly, Sanchez-Sanchez *et al.*[32] synthesized metallo-folded SCNPs under mild conditions *via* metal coordination with Cu(II) ions. The formation of SCNPs was confirmed through size exclusion chromatography (SEC), multi-angle laser scattering (MALLS), and small-angle neutron scattering (SANS), which demonstrated that metal complexation served as the cross-linking mechanism.

In this work, we report the synthesis of linear random P(S-*r*-4VP) copolymer chains *via* RAFT polymerization, using 4-vinylpyridine as the precursor crosslinking monomer. Quaternization of the pyridine nitrogen was achieved through reaction with 1,3-propanesultone, leading to the formation of ionic dipoles along the polymeric chain. Intramolecular collapse under dilute conditions in a nonpolar solvent resulted in the formation of single-chain nanoparticles, capable of undergoing shape transformation/reshaping (folding/collapse) in response to the solvent's polarity. To the best of our knowledge, although ionic interactions have been previously utilized in the formation of SCNPs, this study represents the first attempt employing this specific ionic pair and marks an initial step toward exploring ionic self-folding in high molecular weight polymers.

Experimental section

Materials

Styrene (St) (99%, Acros Organics) and 4-vinylpyridine (4VP) (96%, Alfa Aesar) were dried over CaH_2, stirred overnight, vacuum distilled to remove inhibitors, and stored under vacuum. 2,2′-Azobis(isobutyronitrile) (AIBN) (98%, Acros Organics) was recrystallized from methanol and dried under vacuum. 1,3-Propanesultone (98%) and 4-cyano-4-[(dodecylthio)carbonothioylthio]pentanoic acid (CDTPA) (>97.0%, TCI Chemicals) were used as received. Toluene (≥99.8%, Fischer Chemicals) was purified by refluxing over metallic sodium chunks in a round-bottom flask and used as the solvent for dynamic light scattering (DLS) measurements. Tetrahydrofuran (THF) (>99.9%, Fischer Chemicals) was stirred with CaH_2 overnight and distilled under vacuum in a round-bottom flask containing metallic sodium chunks and for high purity, the dried THF was stored under vacuum in a round-bottom flask containing a Na/K alloy (1 : 3 Na/K) and was used to prepare the AIBN and CDTPA solutions. Dimethylformamide (DMF) (≥99.5%, Fischer Chemicals) was used as a polar solvent for the betainization reaction of the tertiary amine of 4-vinylpyridine. Prior to use, DMF was added to a round-bottom flask containing activated molecular sieves 4 Å and left unstirred overnight followed by distillation.

Molecular characterization

Size exclusion chromatography (SEC) was used to determine the M_n and molecular weight distribution values, $Đ_M = M_w/M_n$. The analysis was performed using a system composed of a Waters model 510 pump, a U6K sample injector, a Waters 401 differential refractometer, and a set of 5μ-Styragel columns with a continuous porosity range of 500 to 10^6 Å. $CHCl_3$ was used as the carrier solvent at a flow rate of 1 mL min^{-1}. The system was operated at 40 °C and calibrated with polystyrene standards with molecular weight in the range of 970–600.000 g mol^{-1}.

Dynamic light scattering (DLS) measurements were performed on a Brookhaven Instruments NanoBrook Omni system at a wavelength (λ) of 640 nm and a laser power of 40 mW. Correlation functions were analyzed using Contin software with the cumulant method at a 90° scattering angle. The light source was a 22 mW He–Ne laser from JDS Uniphase. Each concentration was measured five times, and the results were averaged. Prior to measurements, the solutions were passed through Millipore's Millex-LCR hydrophobic poly(tetrafluoroethylene) (PTFE) filters (pore size of 0.22 μm).

Viscometric data were analyzed using the Huggins equation:[33]

$$\eta_{sp}/c = [\eta] + k_H[\eta]^2 c$$

as well as the Kraemer equation:[33]

$$\ln \eta_r/c = [\eta] + k_K[\eta]^2 c,$$

where η_r, η_{sp} and $[\eta]$ are the relative, specific, and intrinsic viscosities, respectively, and k_H and k_K are the Huggins and Kraemer constants, respectively. All measurements were carried out at 25 ± 0.01 °C in a temperature-controlled bath using Cannon-Ubbelohde dilution viscometers equipped with a Schott-Gerate AVS 410 automatic flow timer. Toluene was used as the solvent.

Calorimetric measurements were performed employing a TA Q200 DSC apparatus (TA Instruments, USA). Calibration took place with sapphires for heat capacity and indium for temperature and enthalpy, on samples of ∼5–11 mg in mass closed in Aluminum Tzero pans (TA), in the temperature range of 20 to 220 °C and a nitrogen atmosphere of high purity (99.9995%). In the first heating scan from RT to 180 or 220 °C at 10 °C min^{-1}, the thermal contact between the sample and the pan was optimized, whereas any thermal history was erased and any remaining humidity/solvents had evaporated. The melted samples were then cooled to 20 °C at 10 °C min^{-1} and, subsequently, heated to the maximum temperature at 10 °C min^{-1}.

NMR measurements were carried out on a 400 MHz Bruker Avance Neo instrument, using $CDCl_3$-d at 298 K.

Polymerization of *P*(St-*r*-4VP) *via* RAFT polymerization

4-Cyano-4-[(dodecylthio)carbonothioylthio]pentanoic acid (CDTPA) was used as the chain transfer agent (CTA), and 2,2′-azobis(isobutyronitrile) (AIBN) was used as the radical initiator for the reversible addition fragmentation chain transfer polymerization (RAFT). Solutions of AIBN and CDTPA were prepared in THF to facilitate accurate dosing. Specifically, AIBN (16 mg) was dissolved in 10 mL of THF to yield a 10^{-5} mol mL^{-1} solution, while CDTPA (53 mg) was dissolved in 10 mL of THF to afford a 1.3129×10^{-5} mol mL^{-1} solution. Both solutions were stored at −20 °C until use.

A small, custom-made apparatus was assembled for the copolymerization of styrene (St) and 4-vinylpyridine (4VP), and the polymerization solutions were prepared in separate glass vials. Specifically, 4.4 mL (38.40 mmol) of St, 40.87 μL (0.384 mmol) of 4VP, 146.19 μL (4.44×10^{-3} mmol) of AIBN and 610.50 μL (8.88×10^{-3} mmol) of CDTPA were added using an electronic precision pipette (P1 in Table 1). The resulting solution was stirred for 10 minutes to ensure homogeneity. The apparatus was then connected to the vacuum line and subjected to a three freeze–pump–thaw cycle to degas the solution. The upper end of the glass tube was vacuum sealed using a gas torch and submerged in an oil bath at 85 °C with continuous stirring to facilitate polymerization. After 48 hours, the polymerization was quenched by removing the apparatus from the oil bath and placing it directly under cold running water. The tube was ruptured, and tetrahydrofuran was added to achieve complete solubilization of the polymer mixture. Methanol was used as a non-solvent to facilitate polymer precipitation, upon which the precipitate was dried in the vacuum oven overnight. Based on our previous experience, copolymers containing 4–5 mol% 4-vinylpyridine (4-VP) with ∼100 kg mol^{-1} became partially or completely insoluble upon cross-linking. More precisely, a number of attempts were made in our laboratory to create polymer chains with a higher percentage of 4-VP. However, we encountered challenges, such as the requirement for a significant amount of high-quality polar solvent to fully dissolve the polymer sample following the quaternization procedure. Furthermore,

Table 1 Experimental parameters for the synthesis of P(S-*r*-4VP) by RAFT polymerization[c]

Sample name	St (mmol)	4VP (mmol)	St/4VP[a] (mol ratio)	CDTPA (mmol)	AIBN (mmol)	t (h)	$M_{n,th}$[b] (kg mol^{-1})
P1	38.02	0.38	99/1	8.89×10^{-3}	4.44×10^{-3}	48	300
P2	47.04	0.96	98/2	11.1×10^{-3}	5.55×10^{-3}	47	300
P3	37.24	1.15	97/3	8.89×10^{-3}	4.44×10^{-3}	48	300

[a] Initial polymerization feed molar ratio. [b] Theoretical molecular weight calculated at full monomer conversion. [c] All polymerization reactions were carried out at 85 °C with a [CTA]:[AIBN] molar ratio of 2:1.

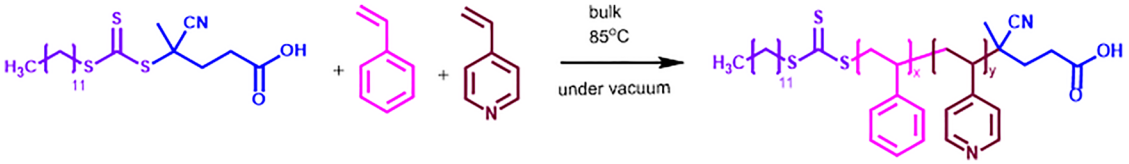

Scheme 2 RAFT copolymerization of styrene and 4-vinylpyridine.

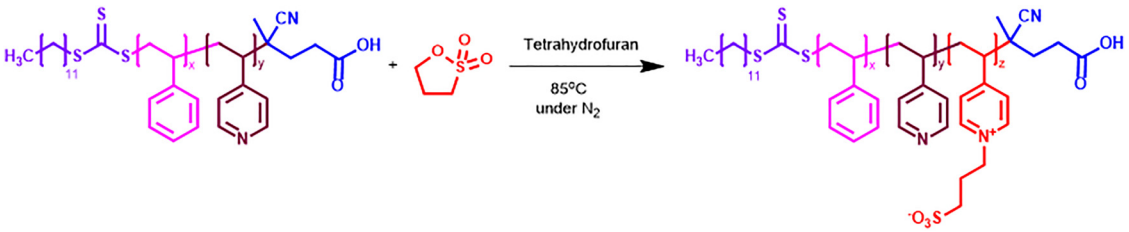

Scheme 3 Quaternization of pyridine nitrogen for the introduction of ionic dipoles into the polymeric chain.

even when the polymer sample became soluble in the polar solvent during the crosslinking process, the sample instantly formed aggregation phenomena and its solubility in a good non-polar solvent to isolate nanoparticles was ineffective. In order to balance functionalization and solubility, a series of polymerization reactions was carried out with 4-VP molar ratios ranging from 1% to 3% to investigate the effect of monomer content on the extent of intramolecular cross-linking (Table 1). Bulk conditions were maintained during polymerization to promote viscosity increase and limit termination reactions (Scheme 2).

Introduction of ionic dipoles in random copolymer P(S-*r*-4VP) and intramolecular cross-linking in a nonpolar solvent

The introduction of ionic dipoles occurred after the reaction of 1,3-propanesultone (1,3-PS) with 4-vinylpyridine nitrogen.[34] Quaternization of pyridine nitrogen took place under inert gas flow, as 1,3-propanesultone is hygroscopic (Scheme 3). Specifically, 730 mg of the P1 polymer (5.75×10^{-6} mol), 20 mL of freshly distilled dimethylformamide, and a Teflon stirrer were added to a two-necked round-bottom flask. The solution was stirred under nitrogen gas flow for 30 minutes to ensure complete polymer dissolution (run 1, Table 3). Subsequently, 119 mg (0.98×10^{-3} mol) of 1,3-propanesultone was added, and the mixture was heated in a silicone oil bath at 85 °C where it remained under stirring for 18 hours.

Upon completion of the reaction, the solvent was removed by distillation using a vacuum line. The polymer was then dissolved in a minimal volume of DMF, precipitated into cold methanol and thoroughly washed with methanol to remove any unreacted 1,3-propanesultone. The polymer remained overnight in the vacuum oven at 50 °C. Successful introduction of the 1,3-propanesultone groups was confirmed using ^{1}H-NMR spectroscopy, which also verified that the polymer was sufficiently dry for the subsequent intramolecular networking process.

The intramolecular cross-linking reaction was carried out under high dilution to favor single-chain folding (Fig. 1). Due to the presence of ionic dipoles, the polymer samples were first dissolved in the minimum possible quantity of a polar solvent

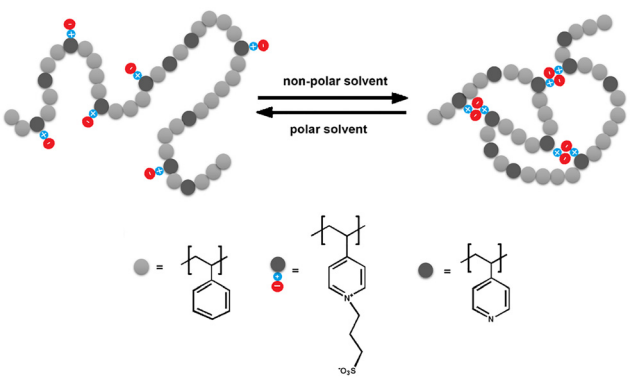

Fig. 1 Representation of intramolecular cross-linking through ionic interactions. Depending on the polarity of the solvent, the chain has the ability to collapse and reshape.

and then added dropwise to a nonpolar solvent, where intramolecular cross-linking occurred. Tetrahydrofuran and toluene were selected as polar and nonpolar solvents, respectively. Tetrahydrofuran has a lower boiling point (T_b = 66 °C) than toluene (T_b = 110.6 °C), so the polar solvent was preferably removed during the solvent evaporation process to recover the cross-linked polymer network. The cross-linked polymer was precipitated in cold hexane, a non-solvent, to minimize sample loss during isolation and finally dried overnight in a vacuum oven.

Results and discussion

RAFT polymerization was employed to synthesize copolymers of styrene and 4-vinylpyridine. Both monomers belong to the class of more activated monomers (MAMs), making CDTPA an appropriate chain transfer agent (CTA) because of its trithiocarbonate group combined with a cyano substituent, which acts as an electron acceptor. The copolymerization of styrene (St) and 4-vinylpyridine (4-VP) was intentionally selected due to their pronounced chemical and structural homology. This similarity manifests in closely matched reactivity ratios ($r_{4\text{-VP}}$ = 0.70 and r_{St} = 0.34), determined *via* the extended Kelen-Tüdos method, which, as demonstrated in prior studies, favors the synthesis of random copolymers over stepwise or pseudo-block copolymers.[35] Polymerization was carried out under bulk conditions to enhance the interactions between the growing polymer chains and monomer units, thereby promoting molecular weight growth as viscosity increased. Preliminary experiments (results not shown) showed that higher molar ratios of chain transfer agent (CTA) to initiator (AIBN) did not yield polymers of the desired molecular weight, as the degree of polymerization (DP) remained limited under such conditions. Although decreasing the CTA/AIBN molar ratio inevitably leads to a partial loss of control in RAFT polymerization, this adjustment was necessary to achieve the targeted DP and ensure a sufficient chain length for subsequent intramolecular folding and nanoparticle formation. To mitigate such effects, higher polymerization temperatures were employed to promote a faster initiation step, while overall monomer conversions were deliberately kept low to minimize end-group loss resulting from CTA degradation. As will be discussed, the polydispersity indices ($Đ$) obtained in this work, although slightly higher than those typically reported for controlled radical polymerization, are still indicative of a well-regulated process. Under optimized conditions (CTA/AIBN = 2 : 1), the reaction proceeded efficiently, producing copolymers with relatively narrow molecular weight distributions ($Đ \leq 1.35$). These findings demonstrate that CDTPA provided reliable control over the RAFT mechanism, allowing the preparation of uniform copolymers suitable for subsequent intramolecular collapse into SCNPs.

Size exclusion chromatography (SEC) was used to determine the molecular weight and polydispersity of the samples (Fig. S1, SI). As shown in Table 2, all samples exhibited similar molecular weights and polydispersity indices, consequently leading to nearly identical elution volumes and overlapping chromatograms. Notably, the chromatograms exhibit tailing at the end of the elution, resulting in asymmetric peaks. This behavior is consistent with the elevated initiator concentration, which likely caused some early termination events at the onset of polymerization.

Table 2 Molecular characteristics of P(S-*r*-4VP) random copolymers

Sample name	M_w[a] (kg mol^{-1})	M_n[a] (kg mol^{-1})	PDI[a]	Yield[b] (wt%)	M_v[c] (kg mol^{-1})	4VP%[d]
P1	140	104	1.35	26	127	1
P2	130	105	1.23	30	105	3
P3	140	112	1.26	25	127	4

[a] Determined by SEC calibrated with PS standards and $CHCl_3$ as an eluent solvent at 40 °C. [b] Determined by gravimetry. [c] Determined by viscometry with toluene as solvent at 25 °C. [d] Determined by ^{1}H-NMR spectroscopy in $CDCl_3$.

The composition of 4-vinylpyridine units in the copolymer was determined from the ^{1}H-NMR spectrum. As reported in the literature,[36,37] the ortho-proton signals of non-quaternized pyridine resonate in the range of 8.48–8.09 ppm, whereas quaternization of the pyridine ring shifts these signals to higher ppm values. In the ^{1}H-NMR spectra of the post-polymerization samples, the ortho-aromatic protons of the 4-VP monomer appear at higher chemical shifts than those in the resulting polymer, confirming the absence of the residual monomer. Thus, the resonance above 8.5 ppm can be assigned to the ortho protons of non-quaternized pyridine units in the polymer. As shown in Fig. S2, the splitting of the peak corresponding to the two ortho protons adjacent to the nitrogen atom of 4-vinylpyridine is distinctly observable at 8.35 ppm. This allows for accurate calculation of the percentage of pyridine incorporated into the polymer chain, which closely matches the initial monomer feed ratio. Moreover, after the incorporation of 1,3-propanesultone into the polymer chain, the ratio of reacted 4-VP units to those lacking an ionic dipole could be determined. The ^{1}H-NMR spectra of the samples following the introduction of ionic dipoles are depicted in Fig. 2 and Fig. S5 and S6. Proton peak b of the 1,3-propanesultone group at 4.84 ppm is distinct and allows for integration of the peaks of the protons located at the ortho position from the pyridine nitrogen.

Similar to other functional polymers, polymeric betaines can be synthesized through two main approaches: (1) polymerization of zwitterionic monomers or (2) zwitterionic functionalization of reactive precursor polymers. Each method offers distinct advantages and limitations. Direct polymerization of zwitterionic monomers yields polymers with complete (100%) betaine functionality, but their molecular characterization can be challenging due to the strong interactions with extraneous materials, such as chromatographic columns, rendering reliable GPC analyses exceedingly difficult, if not impossible. On the other hand, polymerization of precursor monomers is generally more straightforward, producing reactive polymers with tunable molecular properties that are easier to analyze. However, during the chemical functionalization to the betaine form, neighboring group effects may complicate kinetics, and achieving a

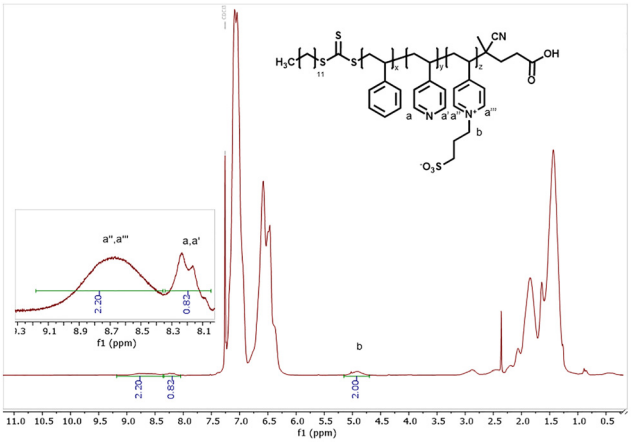

Fig. 2 ^{1}H-NMR spectrum of sample $P2_{zw}$ at 25 °C in $CDCl_3$.

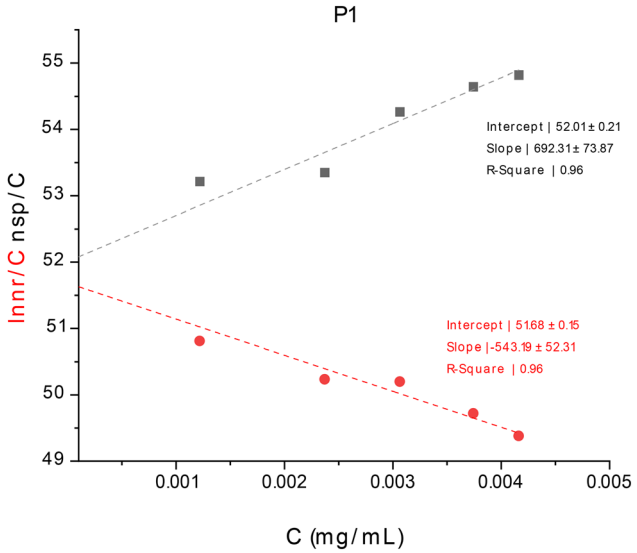

Fig. 3 Viscosity plots of the P1 copolymer at 25 °C in toluene: (●) Huggins plot and (●) Kraemer plot.

100% conversion is not always possible.[20] In this study, the latter approach was selected because the primary objective was the synthesis of well-defined polymers with a narrow molecular weight distribution rather than maximizing ionic dipole incorporation along the polymer chain.

During the quaternization reaction of 4-vinylpyridine, an excess amount of 1,3-propanesultone was added, with the expectation that more ionic dipoles would be introduced into the P3 polymer, which contains a higher content of 4VP monomeric units. However, the ^{1}H-NMR spectra of the samples $P1_{zw}$, $P2_{zw}$, and $P3_{zw}$ (Fig. 2 and Fig. S5 and S6) indicate that the majority of ionic dipoles were incorporated into $P2_{zw}$, as evidenced by the quaternized 4VP (Q4VP) to non-quaternized 4VP ratio of 2.2/0.82. In contrast, the corresponding ratios for $P1_{zw}$ and $P3_{zw}$ are 2/5, and 2/6, respectively. Based on these findings, the last column of Table 3 presents the calculated absolute number of Q4VP to 4VP monomeric units for each linear random copolymer.

Incomplete introduction of ionic dipoles along the polymer chains can be attributed to several factors. Although all reactions were carried out for the same duration, longer reaction times might have promoted more uniform functionalization. The low content of 4-VP units, their random distribution along the polymer chain, and the overall chain conformation further limit reaction efficiency. In chains containing neighboring 4-VP units, functionalization to the betaine form may involve complex kinetics, making full conversion difficult under the conditions employed.

$P1_{zw}$, $P2_{zw}$ and $P3_{zw}$ samples were first fully dissolved in THF solvent, a suitable polar solvent for the samples, in order to accomplish intramolecular crosslinking. In order to prevent the ionic dipoles of the same chain from interacting with nearby chains during crosslinking at very high dilution, this step ensures that the chains are fully dissolved before being added to the non-polar solvent. In particular, crosslinking was performed at C_1 = 0.24 mg mL^{-1} for P1′ (SCNP) (n = 5.75 × 10^{-6} mol and V_{THF} = 13 mL), C_2 = 0.18 mg mL^{-1} for P2′ (SCNP) (n = 4.72 × 10^{-6} mol and V_{THF} = 15 mL), and C_3 = 0.20 mg mL^{-1} for P3′ (SCNP) (n = 4.72 × 10^{-6} mol and V_{THF} = 12 mL).

Viscometry measurements were performed to compare the viscosity of the linear precursor chain with that of the resulting single-chain polymer nanoparticles. As expected, the nanoparticles exhibited lower viscosity, reflecting their more compact structure compared to the free linear chains, indicating successful intramolecular networking. The Huggins and Kraemer equations for the measured polymer samples are depicted in Fig. 3 and 4 and Fig. S7–S10 (SI). Notably, the plots for P1′, P2′, and P3′ deviate from typical viscometry curves. This deviation is attributed to the presence of extremely small particles in the solution, especially in the case of P2′, where the viscosity difference between the solvent and the sample is minimal. Intrinsic viscosity, [η], and Huggins and Kraemer constants, k_H and k_K, can be determined from the Huggins and Kraemer plots by extrapolating to zero concentration and analyzing the slope of the lines, respectively. The viscometric molecular weight, M_v, of the linear copolymers (P1, P2, and P3) was calculated using

Table 3 Experimental parameters for the insertion of 1,3-propanesultone groups into polystyrene chains

Sample name	$n_{polymer}$ (×10^{-6} mol)	n_{4VP} (×10^{-5} mol)	$n_{1,3\text{-PS}}$ (×10^{-3} mol)	Molar ratio Q4VP/4VP[a]	Absolute number of Q4VP/4VP[b]
$P1_{zw}$	5.75	6.89	0.98	2/5	4/11
$P2_{zw}$	5.38	9.68	1.29	2.2/0.82	18/6
$P3_{zw}$	4.76	17.14	0.82	2/6	11/31

[a] Molar ratio of quartenized 4VP to non-quaternized 4VP determined by ^{1}H-NMR. [b] Absolute number of monomer units determined by ^{1}H-NMR.

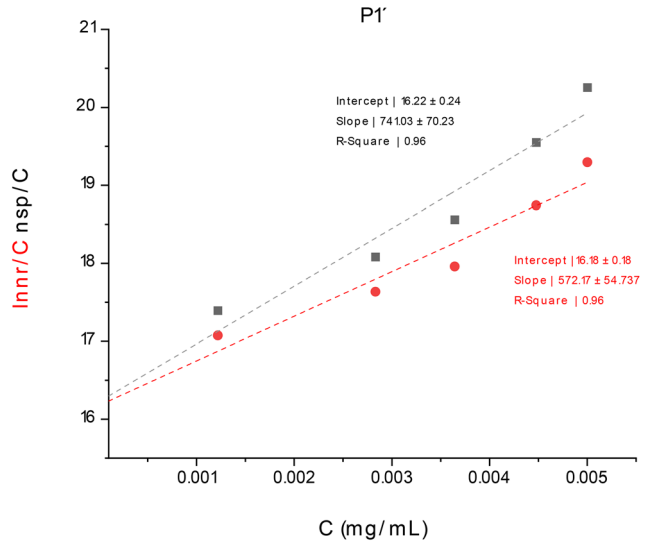

Fig. 4 Viscosity plots of P1′ single-chain nanoparticles at 25 °C in toluene: (●) Huggins plot and (●) Kraemer plot.

the Mark–Houwink–Sakurada equation: $[\eta] = KM_v^a$. For polystyrene homopolymers in toluene at 25 °C, literature values for the constants are available. According to Fetters and coworkers, the equation for this system is $[\eta] = 9.27 \times 10^{-3}\ M^{0.734}$, where $K = 9.27 \times 10^{-3}$ and $a = 0.734$.[38] The 4VP monomer has a hydrodynamic volume comparable to styrene and is incorporated at a low molar fraction (1–3 wt%) along the polymer chain. Therefore, this equation can also be applied to the copolymers studied in this work.

A significant decrease in the intrinsic viscosity was observed for samples P1′ and P2′, while the difference between samples P3 and P3′ was comparatively smaller, as shown in Table 4. The substantial reduction for polymer P2′ is in agreement with expectations, since its ^{1}H-NMR spectrum revealed numerous available crosslinking sites, suggesting the possibility of more extensive crosslink networks in this nanoparticle. Polymer–polymer interactions are more pronounced in cross-linked networks than in linear chains, which impacts the value of the k_H constant after network formation. For polymers in a good solvent (*e.g.* PS in toluene), the Huggins constant, k_H, is typically close to 0.3 and reflects polymer–solvent interactions. k_H is also highly sensitive to aggregation phenomena or to structural features, such as branching and crosslinking, within the macromolecule. Consequently, the k_H values of the networked samples are logically much higher. The formation of crosslinks within the polymer chain reduces its flexibility; thus, as the number of cross-links increases, the k_H also increases, consistent with the experimental findings.

Dynamic light scattering measurements were performed at a 90-degree angle and 25 °C in toluene, a well-known nonpolar solvent suitable for both the linear polymer chains and the corresponding nanoparticles. Measurements were carried out over a concentration range of 0.53–5.93 × 10^{-3} mg mL^{-1}. The hydrodynamic radius (R_h) was determined using the following equation:

$$R_h = k_B T/6\pi\eta_o D_{o,app}$$

where k_B is the Boltzmann constant, T is the absolute temperature, and η_o is the viscosity of the solvent.

The constant k_D is related to the polymer–solvent system and temperature, as shown by the following equation:

$$k_D = 2A_2M - k_f - u$$

where A_2 is the second virial coefficient, M is the molecular weight, u is the specific molar volume of the polymer, and k_f is the coefficient of the concentration dependence of the friction coefficient. k_D is a dynamic interaction parameter that encompasses both thermodynamic interactions, reflected in A_2, and hydrodynamic interactions, represented by k_f.

Constant k_D was determined by dynamic light scattering measurements through the following equation:

$$D = D_0(1 + k_D C),$$

where D is the diffusion coefficient at polymer concentration C and D_0 is the diffusion coefficient at infinite dilution. The value of k_D is extracted directly from the slope of a linear fit of D as a function of C.

Values of the hydrodynamic radius (R_h), diffusion coefficient (D), and k_D constant are summarized in Table 5. The reduction of the hydrodynamic radius for samples P1′, P2′, and P3′ in relation to their linear counterparts shows that intramolecular chain collapse occurred in all three samples, as expected, along with an increase in the diffusion coefficient due to the smaller particle size in solution. All measurements were performed at dilute concentrations to minimize potential intermolecular cross-linking reactions, especially for sample P3, the linear analog bearing the highest density of ionic dipoles along its macromolecular backbone. When cross-linking occurs intramolecularly, between ionic groups within the precursor linear chain, leading to nanoparticle formation, the hydrodynamic

Table 4 Characteristics of the linear and the corresponding polymers after the intramolecular collapse reaction, as determined by viscometry measurements in toluene at 25 °C

Sample name	M_v (kg mol^{-1})	$[\eta]$ (mL mg^{-1})	k_H
P1	127	51.85	0.22
P2	105	45.23	0.29
P3	127	51.66	0.25
P1′	127	16.20	2.82
P2′	106	8.42	9.18
P3′	127	44.08	1.77

Table 5 Results from DLS measurements in toluene at 25 °C

Sample name	R_h (nm)	D_o (× 10^{-7} cm^2 × s^{-1})	k_D (mL mg^{-1})	(μ_2/Γ)
P1	9.0	4.25	32.4	0.16
P1′	7.2	5.35	−410	0.28
P2	8.7	4.48	27.7	0.21
P2′	6.4	6.15	−503.7	0.24
P3	9.5	4.14	−47.3	0.18
P3′	7.0	5.56	−547.1	0.22

Table 6 Results from DLS measurements in DMF at 25 °C

Sample name	R_h (nm)	D_o ($\times 10^{-7}$ cm^2 $\times$ s^{-1})	k_D (mL mg^{-1})	(μ_2/Γ)
P1	9.1	3.24	16.10	0.06
P1′	8.2	3.63	222.90	0.09
P2	8.1	3.66	5.30	0.06
P2′	8.3	3.59	44.90	0.10
P3	9.3	3.15	33.30	0.08
P3′	8.9	3.33	12.20	0.07

radius does not change significantly. This is expected since the proportion of the cross-linker is relatively low (1–2%), resulting in negligible differences in the overall particle size. More specifically, for samples P2 and P2′, the intrinsic viscosity decreased significantly, while the hydrodynamic radius showed only a minor reduction according to dynamic scattering measurements. This suggests that the nanoparticles have a compact and spherical structure, as evidenced by the corresponding viscometry results: the k_H increased significantly from 0.09 to 9.18, while the intrinsic viscosity decreased from 45.25 to 8.42. As expected, the k_D constant decreased in the cross-linked samples compared to their linear counterpart, reflecting enhanced chain interactions. Finally, the second moment values, μ_2/Γ, which describe particle size polydispersity, exhibited a slight increase after intramolecular cross-linking, likely due to the formation of SCNPs with varying degrees of cross-linking.

To verify the strong dynamic nature of the nanoparticles formed through their folding mediated by ionic dipoles, complementary dynamic light scattering measurements were performed in dimethylformamide (DMF) using untreated linear polymers (P1, P2, and P3) and the corresponding nanoparticles (P1′, P2′, and P3′). These experiments demonstrate that, under suitable conditions, ionic interactions disassociate, regenerating the precursor linear polymer. As detailed in Tables 5 and 6, the hydrodynamic radii of P1′, P2′, and P3′ in DMF increased substantially compared to those in toluene, underscoring the dynamic nature of the system, wherein chains fold/collapse or unfold in response to solvent polarity, confirming reversible intramolecular crosslinking. Nearly identical radii (Table 6), as evidenced by the close similarity between the radii of the linear precursors and the post-network-collapse forms, were observed in DMF.

Calorimetric studies were also performed on the linear random copolymers P(S-*r*-4VP) and the corresponding single-chain nanoparticles obtained after the cross-linking reaction. The calorimetric glass transition temperatures, T_g, were determined from the second heating scan cycle, after erasing the thermal history, whereas heat flow was normalized to the sample mass. As expected, a slight increase of $\sim$5 °C in T_g values was observed for the SCNPs compared to their linear counterparts. This modest increase is attributed to the relatively low degree of cross-linking, around 2% (Fig. S11, SI), which results from geometrical constraints imposed on the linear P(S-*r*-4VP) precursor chain during the cross-linking process.[39] Previous results have shown that T_g values increase with cross-linking fraction (CrF), though not in a straightforward manner. For a given CrF, the increase of T_g depends strongly on the molecular weight of the precursor polymer. Significant deviations in T_g values were only observed for SCNPs with CrF above 13 wt%, becoming more pronounced as the molecular weight increased.[10]

Conclusions

A series of well-defined linear random copolymers, P(S-*r*-4VP), consisting of a 1–2%mol ratio of 4VP was synthesized. Ionic dipoles were introduced along the polymeric chains *via* the reaction of 1,3-propanesultone with the 4-vinylpyridine monomeric units. Single-chain polymer nanoparticles were formed through intramolecular cross-linking between these ionic dipoles under high-dilution conditions in a nonpolar solvent. Viscometry and dynamic light scattering measurements confirmed the successful formation of single-chain nanoparticles, as evidenced by decreased intrinsic viscosity, reduced hydrodynamic radius and increased Huggins's constant compared to their linear counterparts. The resulting nanoparticles exhibited slightly smaller sizes than the corresponding linear chains, consistent with the low cross-linker content. Calorimetric analysis revealed increased T_g values due to the intramolecular collapse, which imparts slower dynamics within the nanoparticles. The development of single-chain nanoparticles through ionic interactions is particularly noteworthy, as these systems can revert to their linear form through non-invasive processes, such as changes in solvent polarity.

Conflicts of interest

There are no conflicts to declare.

Data availability

The data supporting this article have been included as part of the supplementary information (SI). All supporting characterization data, including NMR spectra, size-exclusion chromatography (SEC) chromatograms, viscometry plots, and differential scanning calorimetry (DSC) data are available in SI. See DOI: https://doi.org/10.1039/d5sm01159k.

References

1 A. M. Hanlon, C. K. Lyon and E. B. Berda, *Macromolecules*, 2016, **49**, 2–14.
2 A. M. Hanlon, I. Martin, E. R. Bright, J. Chouinard, K. J. Rodriguez, G. E. Pantenotte and E. B. Berda, *Polym. Chem.*, 2017, **34**, 5120–5128.
3 A. Sanchez-Sanchez, I. Pérez-Baena and J. A. Pomposo, *Molecules*, 2013, **18**, 3339–3355.
4 A. Nitti, R. Carfora, G. Assanelli, M. Notari and D. Pasini, *ACS Appl. Nano Mater.*, 2022, **5**, 13985–13997.
5 A. E. Izuagbe, V. X. Truong, B. T. Tuten, P. W. Roesky and C. Barner-Kowollik, *Macromolecules*, 2022, **55**, 9242–9248.
6 Y. Shao and Z. Yang, *Prog. Polym. Sci.*, 2022, **133**, 101593.
7 O. Altintas and C. Barner-Kowollik, *Macromol. Rapid Commun.*, 2012, **33**, 958–971.

8 E. Blasco, B. T. Tuten, H. Frisch, A. Lederer and C. Barner-Kowollik, *Polym. Chem.*, 2017, **38**, 5845–5851.
9 R. Chen and E. B. Berda, *ACS Macro Lett.*, 2020, **9**, 1836–1843.
10 P. A. Klonos, N. Patelis, E. Glynos, G. Sakellariou and A. Kyritsis, *Macromolecules*, 2019, **52**, 9334–9340.
11 G. M. ter Huurne, A. R. A. Palmans and E. W. Meijer, *CCS Chem*, 2019, **1**, 64–82.
12 O. Galant, H. B. Donmez, C. Barner-Kowollik and C. E. Diesendruck, *Angew. Chem., Int. Ed.*, 2021, **60**, 2042–2046.
13 D. C. Blackley and H. W. Melville, *Makromol. Chem.*, 1956, **18**, 16–36.
14 S. Mavila, O. Eingi, I. Berkovich and G. Lemcoff, *Chem. Rev.*, 2016, **116**, 878–961.
15 A. Pia, P. Kröger and J. M. J. Paulusse, *J. Controlled Release*, 2018, **286**, 326–347.
16 A. Sanchez-Sanchez and J. A. Pomposo, *Part. Part. Syst. Charact.*, 2014, **31**, 11–23.
17 E. Harth, B. Van Horn, V. Y. Lee, D. S. Germack, C. P. Gonzels, R. D. Miller and C. J. Hawker, *J. Am. Chem. Soc.*, 2002, **124**, 8653–8660.
18 Md. A. R. Khan, Md. A. Habib, J. Naime, Md. M. H. Rumon, M. S. Al Mamun, A. B. M. Nazmul Islam, Md Mahiuddin, K. Md. R. Karim and M. H. Ara, *Res. Chem.*, 2023, **6**, 101160.
19 S. Roh, Y. Nam, M. T. N. Nguyen, J.-H. Han and J. S. Lee, *Molecules*, 2024, **29**, 3261–3290.
20 S. Kudaibergenov, W. Jaeger and A. Laschewsky, *Adv. Polym. Sci.*, 2006, **201**, 157–224.
21 A. Erfani, J. Seaberg, C. P. Aichele and J. D. Ramsey, *Biomacromolecules*, 2020, **21**, 2557–2573.
22 K. Qu, Z. Yuan, Y. Wang, Z. Song, X. Gong, Y. Zhao, Q. Mu, Q. Zhan, W. Xu and L. Wang, *Chem. Phys. Mater.*, 2022, **1**, 294–309.
23 P. Wang, C. Geiger, L. P. Kreuzer, T. Widmann, J. Reitenbach, S. Liang, R. Cubitt, C. Henschel, A. Laschewsky, C. M. Papadakis and P. Műller-Buschbaum, *Lamgmuir*, 2022, **38**, 6934–6948.
24 N. M. Hamelmann and J. M. J. Paulusse, *J. Controlled Release*, 2023, **365**, 26–42.
25 L. Zheng, H. S. Sundaram, Z. Wei, C. Li and Z. Yuan, *React. Funct. Polym.*, 2017, **118**, 51–61.
26 M. E. Mackay, T. T. Dao, A. Tuteja, D. L. Ho, B. Van Horn, H. C. Kim and C. J. Hawker, *Nat. Mater.*, 2003, **2**, 762–766.
27 A. Tuteja, M. E. Mackay, C. J. Hawker and B. Van Horn, *Macromolecules*, 2005, **38**, 8000–8011.
28 A. Einstein, *Ann. Phys.*, 1906, **19**, 289–306.
29 C. Pyromali, N. Patelis, M. Cutrano, M. Gosika, E. Glynos, A. J. Moreno, G. Sakellariou, J. Smrek and D. Vlassopoulos, *Macromolecules*, 2024, **57**, 4826–4832.
30 T. Terashima, T. Sugita, K. Fukae and M. Sawamoto, *Macromolecules*, 2014, **47**, 589–600.
31 M. Artar, E. R. J. Souren, T. Terashima, E. W. Meijer and A. R. A. Palmans, *ACS Macro Lett.*, 2015, **10**, 1099–1103.
32 A. Sanchez-Sanchez, A. Arbe, J. Colmenero and J. A. Pomposo, *ACS Macro Lett.*, 2014, **5**, 439–443.
33 L. H. Sperling, *Introduction to Physical Polymer Science*, 4th edn, John Wiley & Sons Inc., Hoboken, NJ, USA, 2005, chapter 3.
34 L. Wu, J. Jasinski and S. Krishnam, *J. Appl. Polym. Sci.*, 2011, **14**, 2154–2170.
35 E. Yilmaz and Z. Küçükyavuz, *Polymer*, 1993, **34**(1), 145–149.
36 F. Kandelhard, E. Pashayev, J. Schymura and P. Georgopanos, *Ind. Eng. Chem. Res.*, 2023, **62**(22), 8696–8708.
37 D. Gokkaya Ozburun, H. Hancer, B. Findikli, T. Ozbek, M. M. Ozmen and M. Topuzogullari, *Eur. Polym. J.*, 2025, **222**, 113615.
38 L. J. Fetters, N. Hadjichristidis, J. S. Linder and J. W. Mays, *J. Phys. Chem. Ref. Data*, 1994, **23**, 619–640.
39 D. W. Holley, M. Ruppel, J. W. Mays, V. S. Urban and D. Baskaran, *Polymer*, 2014, **55**, 58–65.